Supplementary Information

Accurate background subtraction in STED nanoscopy by polarization switching

Jong-Chan Lee[1,2], Ye Ma[3], Kyu Young Han[4] and Taekjip Ha[2,3,5,*]

[1] Department of New Biology, DGIST, Daegu 42988, Republic of Korea
[2] Department of Biophysics and Biophysical Chemistry, Johns Hopkins University, Baltimore, Maryland, 21205, USA
[3] Department of Biomedical Engineering, Johns Hopkins University, Baltimore, Maryland, 21205, USA
[4] CREOL, The College of Optics and Photonics, University of Central Florida, Orlando, Florida, 32816, USA
[5] Howard Hughes Medical Institute, Baltimore, Maryland, 21205, USA
[*] Corresponding author: tjha@jhu.edu

Supplementary Figures

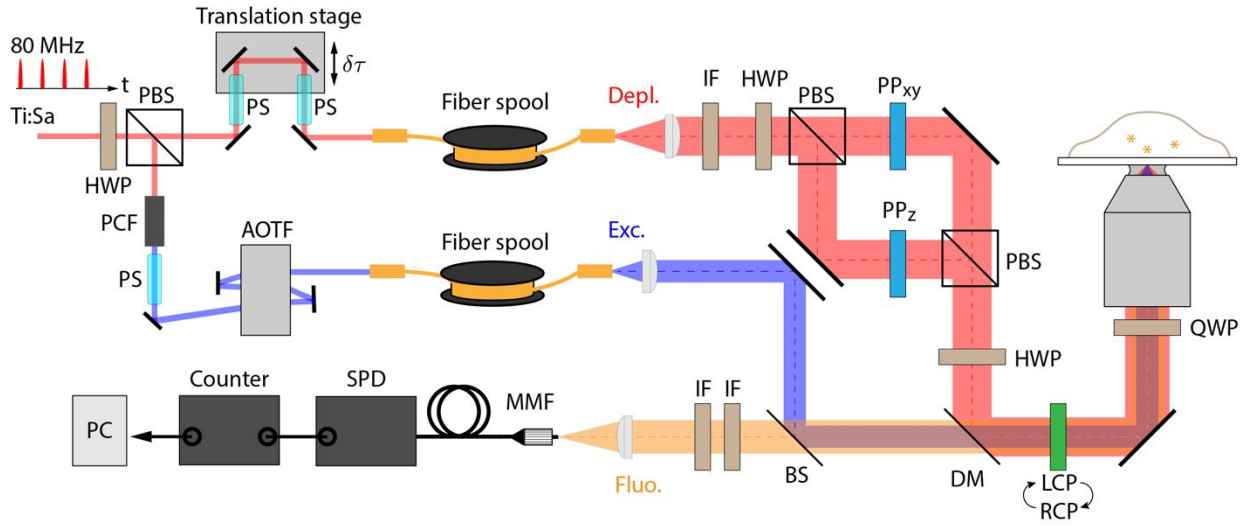

Figure S1. Detailed schematic of the experiment. PBS: polarizing beam splitter, HWP: half-wave plate, QWP: quarter-wave plate, PCF: photonic crystal fiber, PS: pulse stretcher, AOTF: acousto-optic tunable filter, IF: interference filter, PP_{xy} and PP_z: phase plates that generates XY- and Z-STED profile, respectively, DM: dichroic mirror, BS: beam splitter, MMF: multi-mode fiber, SPD: single-photon detector.

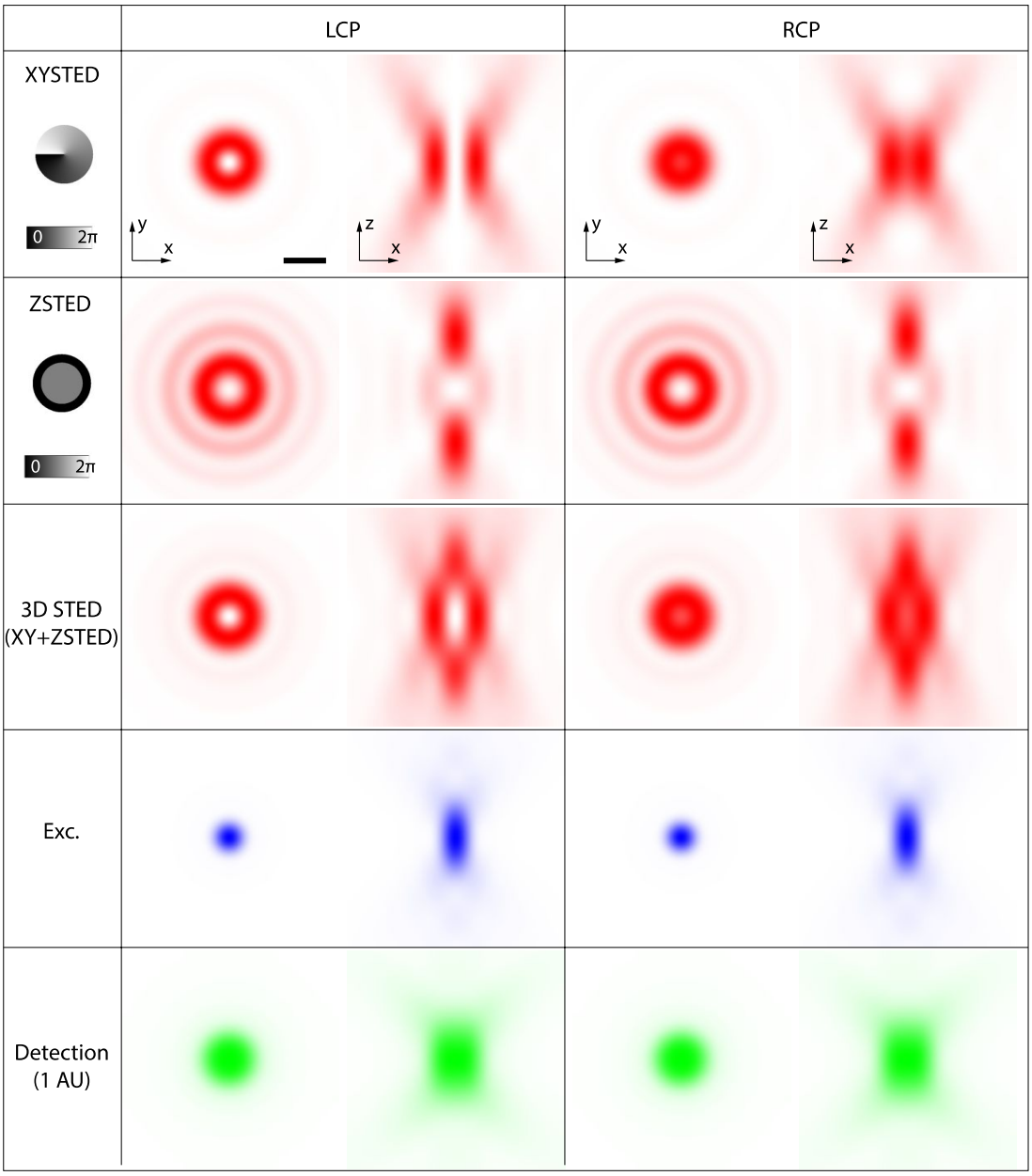

Figure S2. Change of PSF of XY-STED, Z-STED, 3D STED, and Excitation under polarization switching from LCP to RCP. Scale bar: 500 nm.

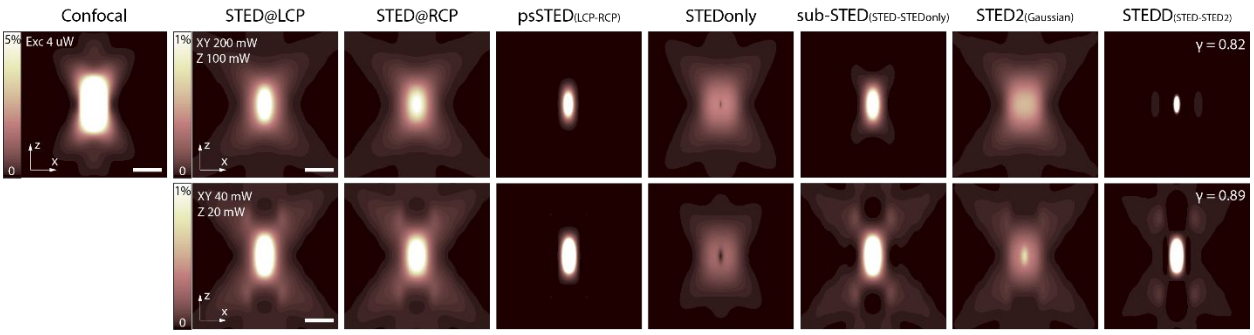

Figure S3. Simulation of detected fluorescence signal from a point fluorophore, i.e. PSF. The fluorescence intensity is calculated by assuming a point fluorophore, quantum yield of excitation = 0.65, pulse period = 12.5 ns, dwelling time = 400 µs, SPCM efficiency = 0.9. The number in color map represents the percent intensity normalized to the maximum intensity across the PSF. Note that STED@RCP and STEDonly PSF are normalized to STED@LCP and not by themselves to avoid misleading interpretation. Equivalently, STED2 PSF is normalized to the PSF with first STED pulse (STED1 PSF) [1] not by itself. The intensity higher than the highest value in the color map appears to be white color. Scale bar: 500 nm.

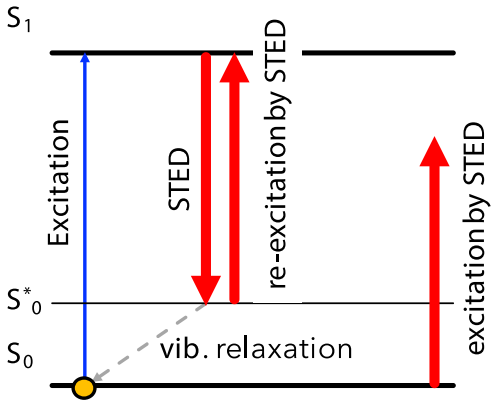

Figure S4. Simplified energy-level diagram of a fluorophore in STED nanoscopy.

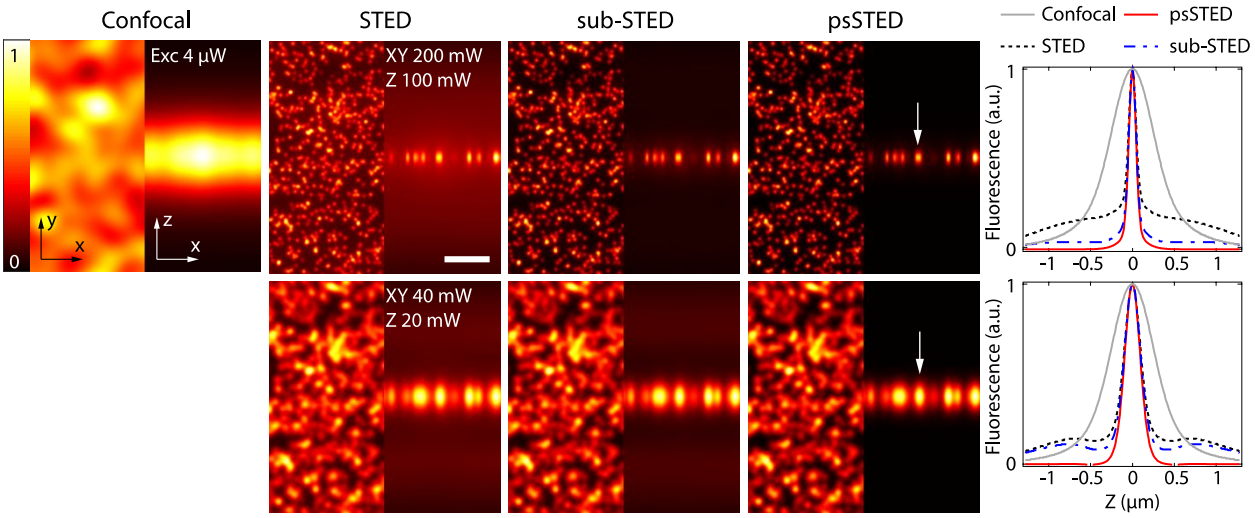

Figure S5. Simulation of fluorescent beads when excitation laser power is 4 µW. Scale bar: 500 nm.

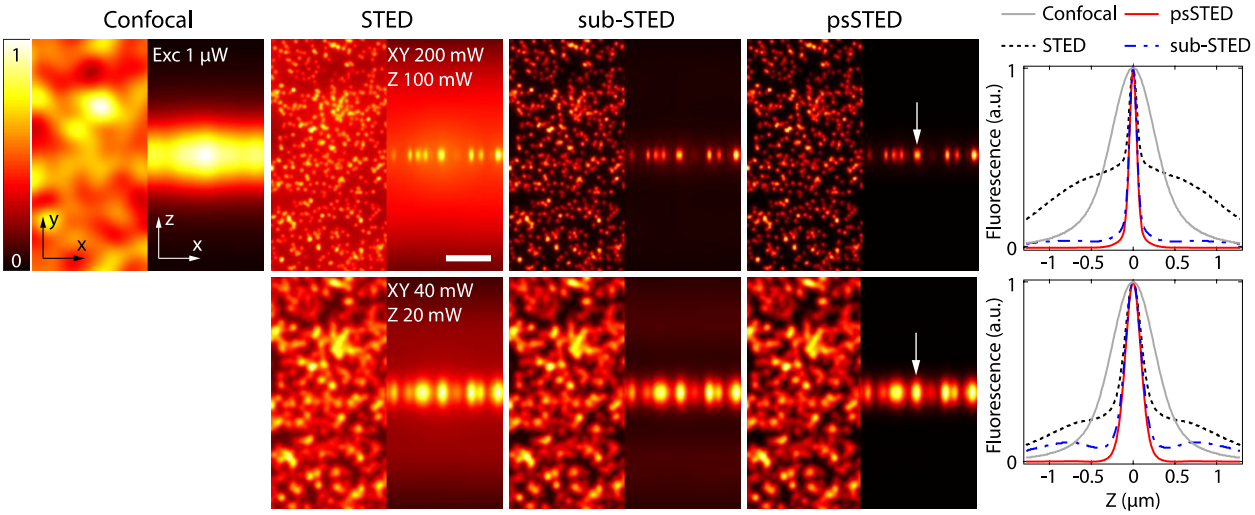

Figure S6. Simulation of fluorescent beads when excitation laser power is 1 µW. Scale bar: 500 nm.

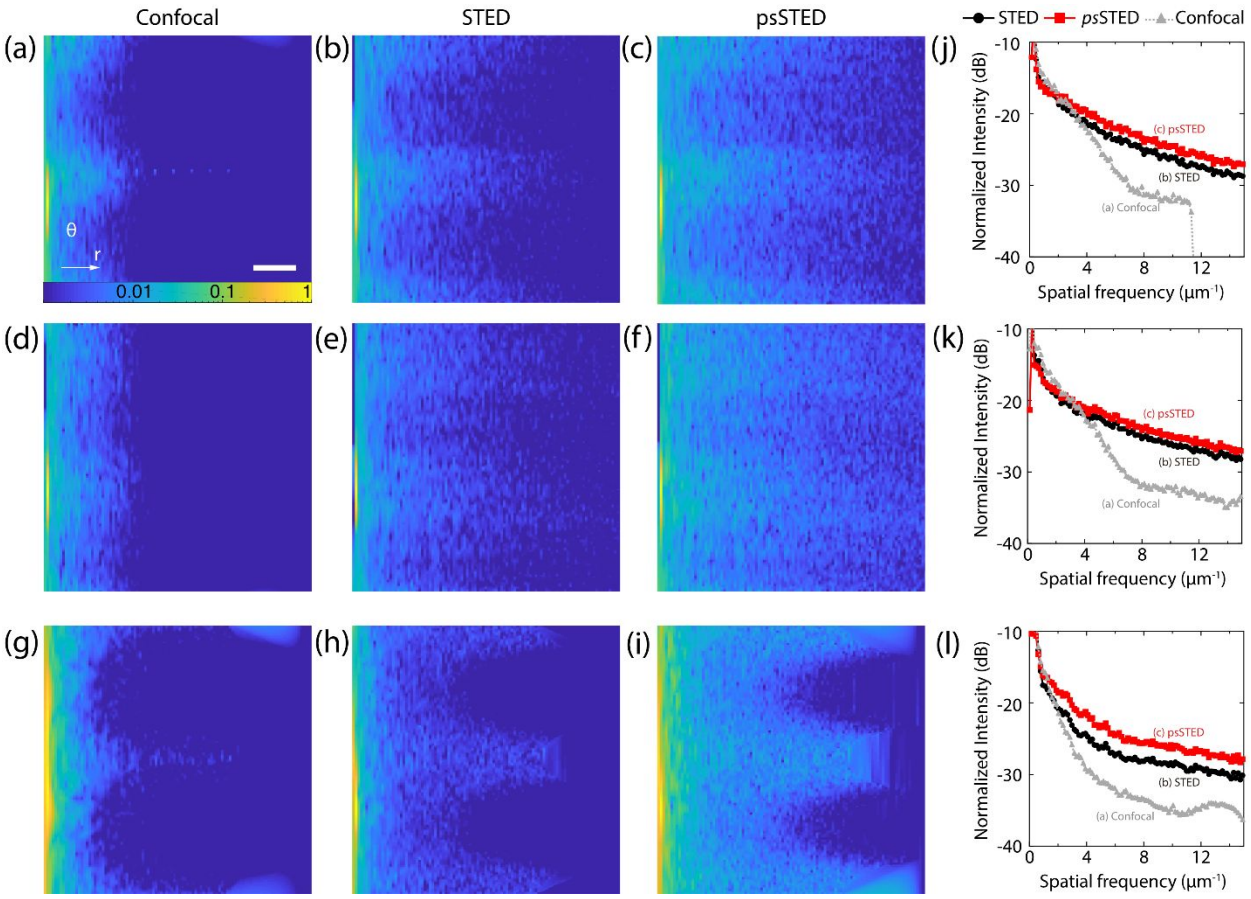

Figure S7. Spatial frequency analysis of the SiR-tubulin labeled 3T3 cell images in Fig. 4. The Fourier transformed image is shown in polar coordinate, in log scale. Images (a)-(i) are the results of Fourier analysis of images Fig. 4(a)-(i). Scale bar: 2.5 μm^{-1}. The intensity as a function of spatial frequency, where the intensity is integrated over θ coordinate, are shown in (j), (k), and (l) for the images (a-c), (d-f), and (g-i), respectively.

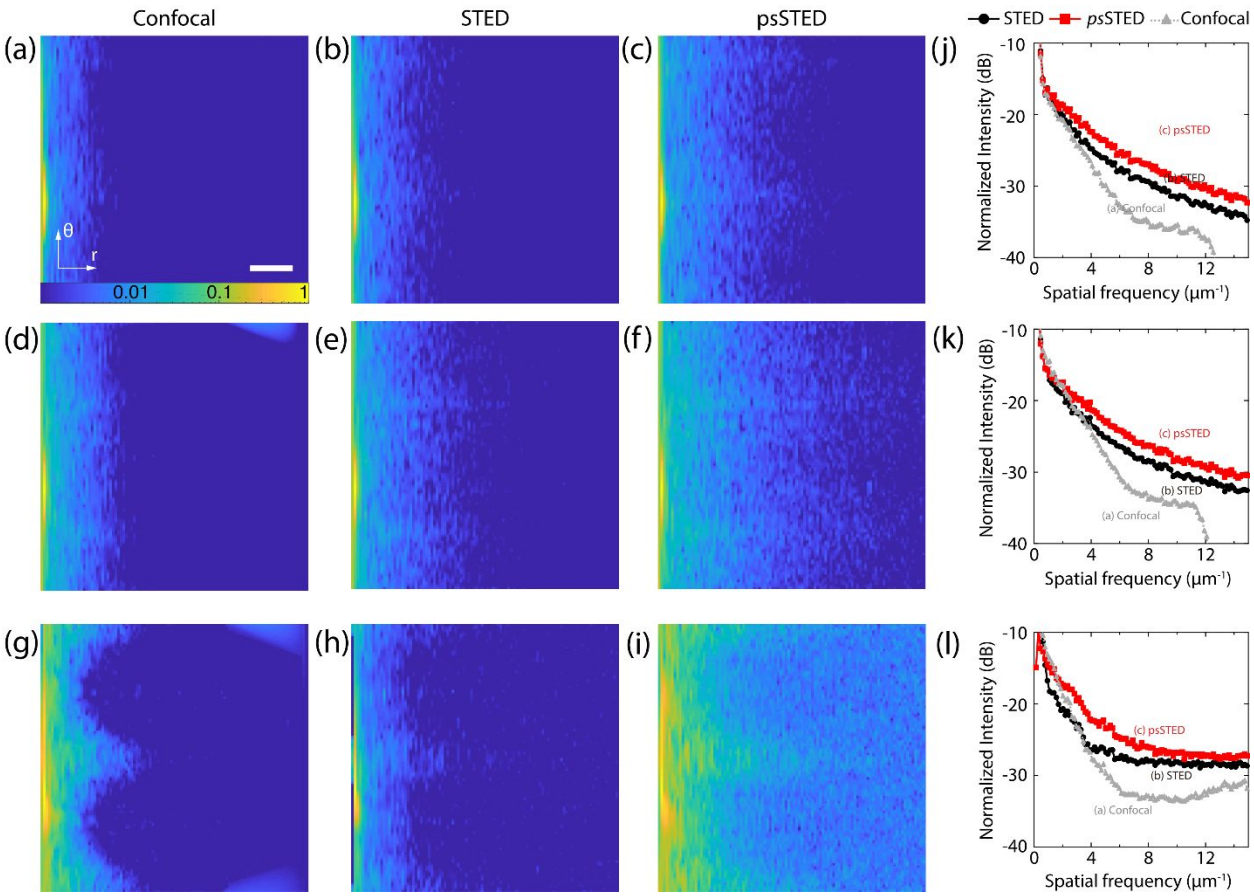

Figure S8. Spatial frequency analysis of the SiR-actin labeled LN229 cell images in Fig. S7. The Fourier transformed image is shown in polar coordinate, in log scale. Images (a)-(i) are the results of Fourier analysis of images Fig. S7(a)-(i). Scale bar: 2.5 μm^{-1}. The intensity as a function of spatial frequency, where the intensity is integrated over θ coordinate, are shown in (j), (k), and (l) for the images (a-c), (d-f), and (g-i), respectively.

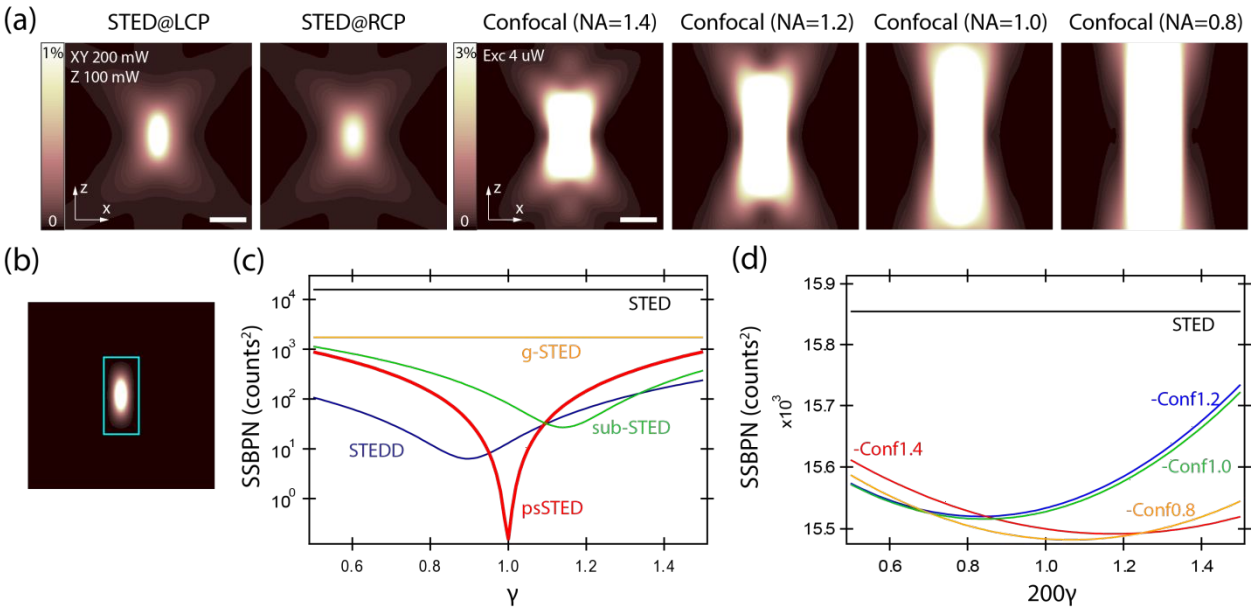

Fig. S9: Comparison of the psSTED performance with confocal subtraction. Confocal subtraction subtracts confocal image from the STED image with varied numerical aperture (NA) from 0.8 to 1.4. (a) Comparison of effective point spread function (PSF). STED@RCP best represents the background of STED@LCP, while confocal PSF does not accurately represent the background. (b) The mean squared background photon number (SSBPN) is calculated from the effective PSF of different subtraction methods except for the center area to exclude signal fluorescence photons. The area excluded in SSBPN calculation is shown in cyan color. (c) SSBPN as a function of subtraction factor γ for different methods is shown for psSTED, subSTED, STEDD, g-STED methods. (d) SSBPN as a function of subtraction factor γ with confocal subtraction method is shown with different NA (1.4, 1.2, 1.0, 0.8). Confocal subtraction method shows little improvement of SSBPN compared to psSTED. The fluorescence intensity is calculated by assuming a point fluorophore, quantum yield of excitation = 0.65, pulse period = 12.5 ns, dwelling time = 400 µs, SPCM efficiency = 0.9. (a) The number in color map represents the percent intensity normalized to the maximum intensity across the PSF. Note that STED@RCP and STEDonly PSF are normalized to STED@LCP and not by themselves to avoid misleading interpretation. Scale bar: 500 nm.

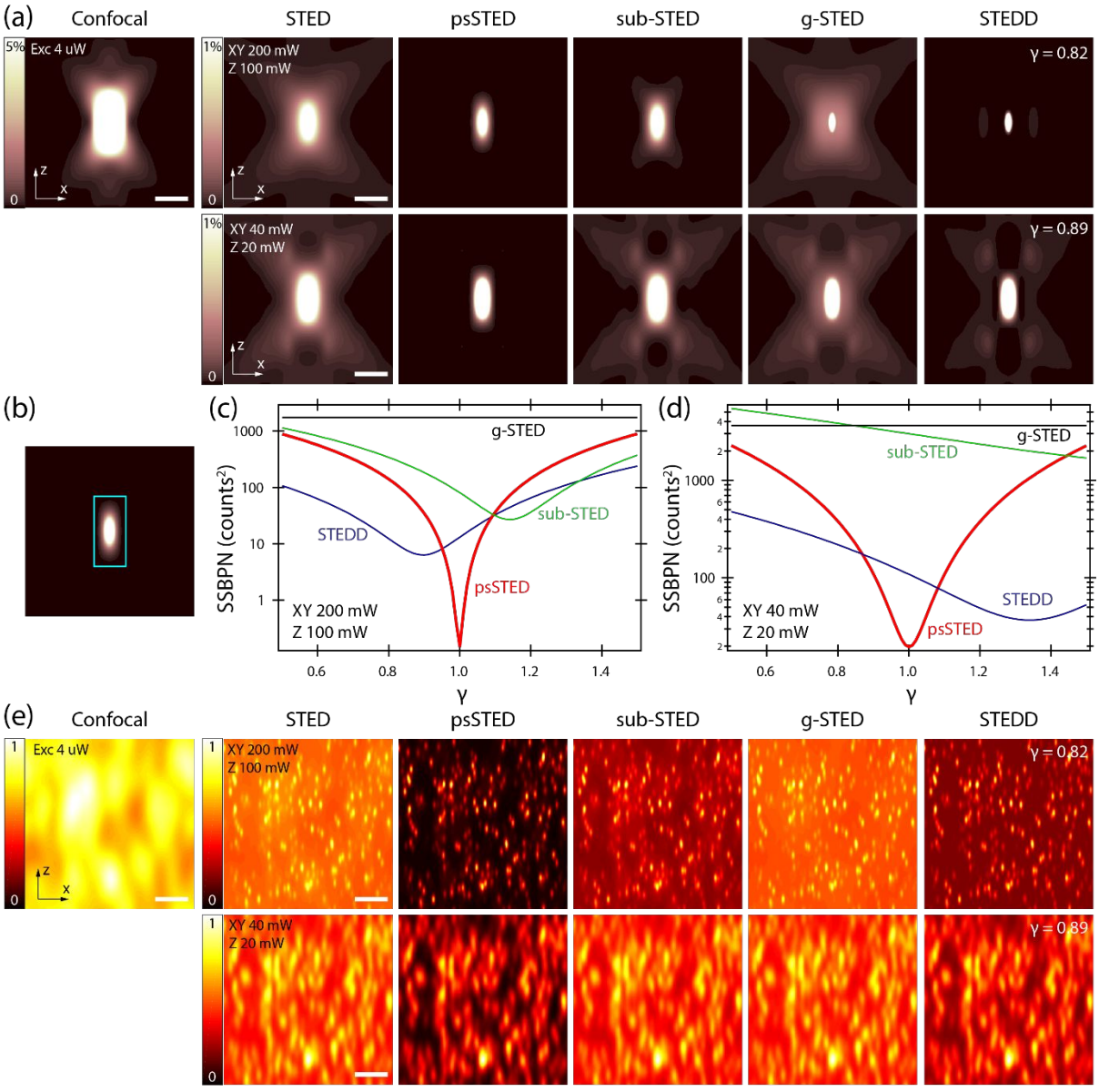

Figure S10. Comparison of psSTED performance with other background suppression methods: STEDD, sub-STED and g-STED at excitation power 4 µW. (a) Comparison of effective point spread function (PSF). The fluorescence intensity is calculated by assuming a point fluorophore, quantum yield of excitation = 0.65, pulse period = 12.5 ns, dwelling time = 400 µs, SPCM efficiency = 0.9. The number in color map represents the percent intensity normalized to the maximum intensity across the PSF. The intensity higher than the highest value in the color map appears as white. Scale bar: 500 nm. (b) The mean squared background photon number (SSBPN) is calculated from the images from (a) except for the center area to exclude signal fluorescence photons. The area excluded in SSBPN calculation is shown in cyan color. SSBPN as a function of subtraction factor γ at high STED power (c) and low STED power (d). (e) Comparison of simulated fluorescent beads. Simulation of 10,000 fluorescent beads are

randomly scattered in 2.56 x 2.56 x 2.56 μm space. The color map is normalized to the maximum intensity of each image. Scale bar: 500 nm.

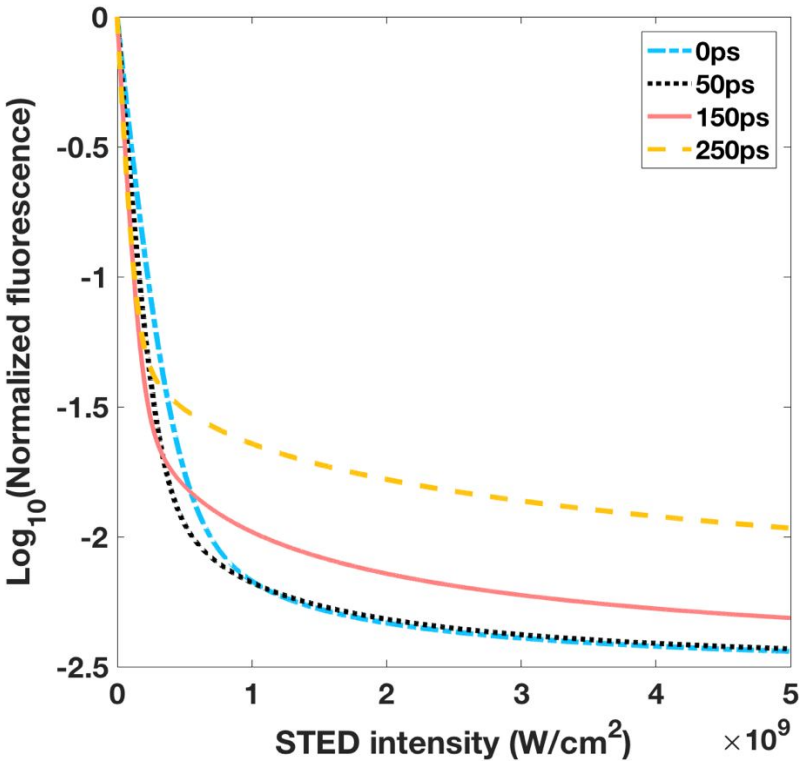

Figure S11. Optimization on the pulse delay from the excitation to the STED pulse. The variance of the normalized detected fluorescence as a function of the STED intensity with different pulse delay is shown. We can see that t_d=150 ps provides us with a good compromise between the depletion efficiency and residue fluorescence, and was applied throughout.

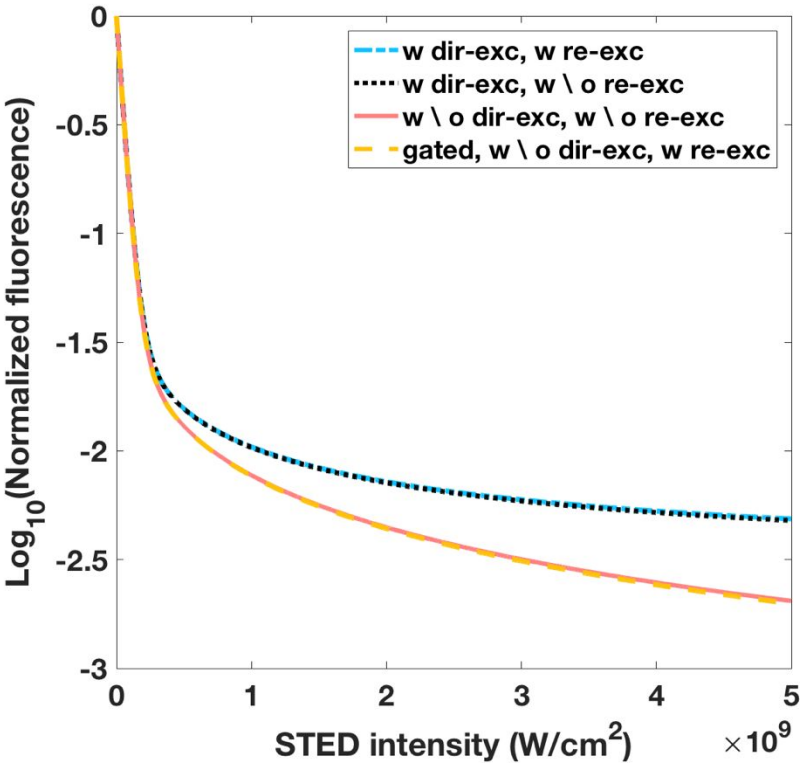

Figure S12: Comparison of the background caused by STED direct excitation and STED re-excitation. When relatively long STED pulse is used (>100 ps), the difference of the fluorescence with or without STED re-excitation is so small compared with the effect caused by STED direct excitation. Thus, the STED re-excitation process is negligible.

Supplementary Text

1. Jablonski diagram model and detectable fluorescence with STED

We assume that the used fluorophore can be regarded as a three-level system with the ground state S0, its higher vibrational sub-level S0* and the electronic excited energy state S1 (Supplementary Fig. S4). When the excitation and STED pulse come to interact with the molecule, the rate equations for the occupancy probability of each state are

$$\frac{dP_{S1}}{dt} = k_{exc}P_{S0} - k_f P_{S1} - k_{STED}P_{S1} + k_{STED}P_{S0^*} + k_{Dir-STED}P_{S0}, \quad \text{(s1)}$$

$$\frac{dP_{S0^*}}{dt} = k_{STED}P_{S1} - k_{vib}P_{S0^*} - k_{STED}P_{S0^*}, \quad \text{(s2)}$$

$$\frac{dP_{S0}}{dt} = -k_{exc}P_{S0} + k_{vib}P_{S0^*} + k_f P_{S1} - k_{Dir-STED}P_{S0}, \quad \text{(s3)}$$

where k_{exc} is the pumping rate by the excitation pulse, k_f is the spontaneous emission rate, k_{STED} is the stimulated emission and re-excitation rate by the STED pulse, $k_{Dir\text{-}STED}$ is the direct excitation rate by the STED pulse, and k_{vib} is the vibration relaxation rate, respectively. Note that we herein, for the first time to the best of our knowledge, clarify the STED-pulse excitation by dividing it into two parts, the re-excitation and direct excitation process. Their corresponding rates are represented as $k_{STED}P_{S0*}$ and $k_{dir\text{-}STED}P_{S0}$, respectively, shown in Eqs. (s1)-(s3).

Considering that the vibration sub-level has a very short lifetime (~0.2 ps), compared with the spontaneous lifetime (at the nanosecond scale) and stimulated emission/re-excitation by the STED pulse, we assume the equilibration of the S0* population:

$$\frac{dP_{S0^*}}{dt} = k_{STED}P_{S1} - k_{vib}P_{S0^*} - k_{STED}P_{S0^*} = 0, \quad \text{(s4)}$$

then we have

$$P_{S0^*} = \frac{k_{STED}}{k_{vib} + k_{STED}} P_{S1}. \quad \text{(s5)}$$

Suppose that

$$P_{S0} + P_{S0^*} + P_{S1} = 1, \quad \text{(s6)}$$

by substituting (s5)-(s6) into (s1), we can obtain a single-variable differential equation in terms of P_{S1}

$$\frac{dP_{S1}}{dt} = -(k_1 + k_2 + k_3)P_{S1} + k_2 \quad , \tag{s7}$$

where

$$k_1 = k_f(1+\gamma) \quad , \tag{s8}$$

$$k_2 = k_{Dir-STED} + k_{exc} \quad , \tag{s9}$$

$$k_3 = k_2 \frac{k_{STED}}{k_{vib} + k_{STED}} \quad , \tag{s10}$$

and

$$\gamma = \frac{k_{STED}}{k_f} \frac{k_{vib}}{k_{vib} + k_{STED}} \quad . \tag{s11}$$

Note that k_1, k_2 and k_3 are time dependent, since

$$k_{exc}(t) = I_{exc}(t)\sigma_{exc}\lambda_{exc} / (hc) \quad , \tag{s12}$$

$$k_{STED/Dir-STED}(t) = I_{STED}(t)\sigma_{STED/Dir-STED}\lambda_{STED} / (hc) \quad , \tag{s13}$$

where $\sigma_{(\bullet)}$ represents the cross section of each process, that is, pumping by the excitation pulse, stimulated emission/re-excitation, and direct excitation by the STED pulse. $\lambda_{(\bullet)}$ is the excitation/STED pulse wavelength. h is the Planck's constant and c is the light velocity. Within one period of the excitation and STED laser, the temporal intensity profiles of the excitation and STED pulses are described as Gaussian functions:

$$I_{exc}(t) = I_{exc-peak} \exp[-(\frac{t - t_0}{\tau_{exc} / 2})^2] \quad , \ 0 \le t < T \tag{s14}$$

$$I_{STED}(t) = I_{STED-peak} \exp[-(\frac{t - t_0 - t_d}{\tau_{STED} / 2})^2] \quad , \ 0 \le t < T \tag{s15}$$

where τ_{exc} and τ_{STED} are the widths of the excitation and STED pulse, respectively, t_0=2 τ_{STED} is the time point of the excitation pulse peak, t_d is the time delay from the excitation to the STED pulse, and T is the period of high repetition Ti:Sa laser.

Considering that Eq. (s7) is a non-stiff differential equation, which means the solution is not sensitive to the step size and doesn't contain drastic oscillations, we can solve it iteratively with a fixed step Δt by

$$P_{S1}(t_n) = P_{S1}(t_{n-1})\exp[-\sum_{i=1}^{3} k_i(t_{n-1})\Delta t] + \frac{k_2(t_{n-1})}{\sum_{i=1}^{3} k_i(t_{n-1})}(1-\exp[-\sum_{i=1}^{3} k_i(t_{n-1})\Delta t]) \quad , \qquad \text{(s16)}$$

where $t_n = n\Delta t$ (n=0, 1, 2, …) and we chose Δt=2ps throughout this work. Since for most types of fluorophores the lifetime is much shorter than T, we suppose the electron(s) to return to the ground state at the beginning of each laser period, or

$$P_{S1}(t_0 = 0) = 0 \quad . \qquad \text{(s17)}$$

The detectable fluorescence in one laser period T is calculated by

$$F_T = \eta \int_0^T k_f P_{S1}(t) Q dt = \eta k_f Q \int_0^T P_{S1}(t) dt \quad , \qquad \text{(s18)}$$

where Q is the quantum yield of fluorophores and η is the overall detection efficiency considering the loss caused by the limited numerical aperture NA of the used objective and photon capture efficiency of the detector (90%):

$$\eta = 2\pi[1-\cos(\sin^{-1}\frac{NA}{n_{oil}})]/(4\pi)\times 0.9 \quad . \qquad \text{(s19)}$$

2. Calculation on the STED point spread function (PSF) and image formation

From Eq. (s18), we know that the effective excitation PSF can be obtained only if the peak intensity distributions of the excitation and STED pulse are determined. We calculate the normalized patterns of the focused excitation and STED spot [$\tilde{I}_{(.)\text{-}peak}(x,y,z)$] by using the Debye-integration based vector diffraction formula with chirp-z transform, and then the peak intensity distribution with $Power_{(.)}$ is obtained by

$$I_{(\cdot)-peak}(x,y,z) = \tilde{I}_{(\cdot)-peak}(x,y,z)\frac{Power_{(\cdot)}}{A}\frac{T}{\tau_{(\cdot)}}\frac{2}{\sqrt{\pi}} \quad , \qquad \text{(s20)}$$

where

$$A = \int \tilde{I}_{(\cdot)-peak}(x,y,z=0)dx\,dy \qquad \text{(s21)}$$

represents the area occupied by the excitation or STED spots at the focal plane [2,3]. Assume the pixel dwelling time $T_{dwelling}$, the excitation PSF is

$$PSF_{exc}(x,y,z) = F_T(x,y,z;Power_{(\cdot)})\frac{T_{dwelling}}{T} \quad . \tag{s22}$$

In confocal-based microscope setups, the final PSF is the product of the excitation PSF and that of the detection part with the pinhole size taken into considerations:

$$PSF(x,y,z) = PSF_{exc}(x,y,z)\times[PSF_{det}(x,y,z)\otimes D(x,y,z)] \quad . \tag{s23}$$

PSF_{det} is the detection PSF for an infinitely small pinhole and calculated using Debye integration given random polarization and approximate inverse cosine intensity distribution at the pupil plane. $D(x,y,z)$ represents the pinhole transmission function (1 Airy unit is used throughout our work) and $\otimes$ is the convolution process.

Given the sample spatial distribution, the final image with different excitation and STED beam power is the convolution between the object structure and the corresponding PSF shown in Eqs. (s22)-(s23), and calculated by using 3D fast Fourier transform.

3. Simulation parameter

For the laser-related parameters, we used the pulse widths of τ_{exc} =100 ps, τ_{STED} =300 ps and laser period of T=12.5 ns throughout this work which are also agree with the experimental setup. For the fluorophore-specific parameters, we used values similar to Ref. [1], which are k_f = 1/(3.5ns), k_{vib} = 1/(0.2ps), σ_{exc} = 5.7E-16 cm^2, σ_{STED} = 0.23E-16 cm^2, while we estimated the direct excitation cross section at the STED wavelength (λ_{STED} =780 nm) as $\sigma_{dir\text{-}STED}$ = 5.7E-21 cm^2, which is an order smaller than Ref. [1], but better fitted with our experimental observations. Note that we also tested the simulation with the parameters exactly equal to Ref. [1] and psSTED in that condition also outperforms STEDD. The quantum yield Q is set as 0.65. We obtained all the simulation images using a NA=1.4 oil-immersion objective with assuming a 400-us dwelling time, while ignoring any blinking or photo-bleaching phenomenon.

The last but critical parameter needed to be determined is the pulse delay t_d from the excitation to the STED pulse. By plotting the depletion efficiency as a function of the STED beam intensity with different pulse delay (Supplementary Fig. S11), we found that t_d=150 ps will provide us with

a good compromise between the depletion efficiency and residue fluorescence, and was applied throughout.

4. Re-examine the effect of STED re-excitation

Historically there had been a confusion between the STED re-excitation and direct excitation background. We herein show that for using a relatively long STED pulse (>100 ps) which is the common case in STED nanoscopy, the STED re-excitation process is negligible.

To examine the effect of STED re-excitation, we "artificially" delete that process and rewrite the rate equations:

$$\frac{dP_{S1}^{\dagger}}{dt} = k_{exc}P_{S0}^{\dagger} - k_f P_{S1}^{\dagger} - k_{STED}P_{S1}^{\dagger} + k_{dir-STED}P_{S0}^{\dagger}, \tag{s24}$$

$$\frac{dP_{S0^*}^{\dagger}}{dt} = k_{STED}P_{S1}^{\dagger} - k_{vib}P_{S0^*}^{\dagger} = 0, \tag{s25}$$

where † denotes that the corresponding value is calculated without the STED re-excitation process. By the same way, we can obtain a single-variant differential equation in terms of $P_{S1}^{\dagger}$:

$$\frac{dP_{S1}^{\dagger}}{dt} = -(k_1^{\dagger} + k_2 + k_3^{\dagger})P_{S1}^{\dagger} + k_2. \tag{s26}$$

The introduced k_2 is the same as given by Eq. (s9), while

$$k_1^{\dagger} = k_f + k_{STED}, \tag{s27}$$

$$k_3^{\dagger} = k_2 \frac{k_{STED}}{k_{vib}}, \tag{s28}$$

which are slightly different from those with STED re-excitation taken into considerations.

The detectable fluorescence without STED re-excitation can be calculated in a similar way as Eqs. (s16)-(s19). As shown in Supplementary Fig. S13, the difference of the fluorescence with or without STED re-excitation is so small compared with the effect caused by STED direct excitation. This is also consistent with the statement in the previous works that stretching pulses can avoid the STED re-excitation problem.

1. P. Gao, B. Prunsche, L. Zhou, K. Nienhaus, and G. U. Nienhaus, "Background suppression

in fluorescence nanoscopy with stimulated emission double depletion," Nat. Photonics **11**, 163–169 (2017).

2. B. Richards and E. Wolf, "Electromagnetic Diffraction in Optical Systems. II. Structure of the Image Field in an Aplanatic System," Proc. R. Soc. A Math. Phys. Eng. Sci. **253**, 358–379 (1959).
3. M. Leutenegger, R. Rao, R. A. Leitgeb, and T. Lasser, "Fast focus field calculations," Opt. Express **14**, 4897–4903 (2006).